HHS Public Access

Author manuscript

ACS Appl Mater Interfaces. Author manuscript; available in PMC 2022 March 06.

Published in final edited form as:

ACS Appl Mater Interfaces. 2017 June 21; 9(24): 20719–20727. doi:10.1021/acsami.7b02575.

One-Step Facile Synthesis of Highly Magnetic and Surface Functionalized Iron Oxide Nanorods for Biomarker-Targeted Applications

Anamaria Orza[†,‡], **Hui Wu**[†,‡], **Yaolin Xu**[†,‡], **Qiong Lu**[†,§], **Hui Mao**[*,†,‡]

[†]Department of Radiology and Imaging Sciences, Emory University School of Medicine, Atlanta, Georgia 30329, United States

[‡]Center for Systems Imaging, Emory University School of Medicine, Atlanta, Georgia 30329, United States

[§]Department of Pharmacy, The Second Xiangya Hospital of Central South University, Changsha, Hunan 410011, P. R. China

Abstract

We report a one-step method for facile and sustainable synthesis of magnetic iron oxide nanorods (or IONRs) with mean lengths ranging from 25 to 50 nm and mean diameters ranging from 5 to 8 nm. The prepared IONRs are highly stable in aqueous media and can be surface functionalized for biomarker-targeted applications. This synthetic strategy involves the reaction of iron(III) acetylacetonate with polyethyleneimine in the presence of oleylamine and phenyl ether, followed by thermal decomposition. Importantly, the length and diameter as well as the aspect ratio of the prepared IONRs can be controlled by modulating the reaction parameters. We show that the resultant IONRs exhibit stronger magnetic properties compared to those of the widely used spherical iron oxide nanoparticles (IONPs) at the same iron content. The increased magnetic properties are dependent on the aspect ratio, with the magnetic saturation gradually increasing from 10 to 75 emu g^{-1} when increasing length of the IONRs, 5 nm in diameter, from 25 to 50 nm. The magnetic resonance imaging (MRI) contrast-enhancing effect, as measured in terms of the transverse relaxivity, r_2, increased from 670.6 to 905.5 mM^{-1} s^{-1}, when increasing the length from 25 to 50 nm. When applied to the immunomagnetic cell separation of the transferrin receptor (TfR)-overexpressed medulloblastoma cells using transferrin (Tf) as the targeting ligand, Tf-conjugated IONRs can capture 92 ± 3% of the targeted cells under a given condition (2.0×10^4 cells/mL, 0.2 mg Fe/mL concentration of magnetic materials, and 2.5 min of incubation time) compared to only 37 ± 2% when using the spherical IONPs, and 14 ± 2% when using commercially available magnetic beads, significantly improving the efficiency of separating the targeted cells.

[*]**Corresponding Author:** hmao@emory.edu. Tel: (404) 712-0357. Fax: (404) 712-5689.

Supporting Information

The Supporting Information is available free of charge on the ACS Publications website at DOI: 10.1021/acsami.7b02575.

Average size measurements for reported IONRs and spherical IONPs; MTT measurements of the cytotoxicity of reported IONRs (PDF)

The authors declare no competing financial interest.

Graphical Abstract

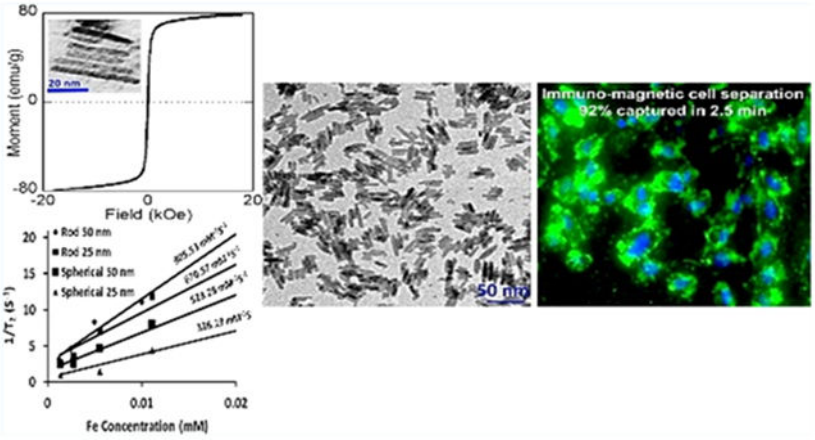

Keywords

iron oxide; nanorods; facile synthesis; surface functionalization; targeting; magnetic cell separation; magnetic resonance imaging

1. INTRODUCTION

Magnetic nanoparticles have been developed for a number of biomedical applications, including MRI contrast enhancement,[1–3] immunomagnetic separations,[4,5] hyperthermia therapies,[6–8] and drug delivery,[9–12] due to their desirable properties of (a) biocompatibility and chemical stabilities, (b) high saturation magnetization to provide maximum performance, (c) large surface areas for binding or loading bioactive or functional moieties, and (d) reliable dispersion in liquid or fluid media.[13] Recently, a great deal of attention and research effort has been directed into the synthesis and study of magnetic nanoparticles with shape[14–16] and size-dependent[17–19] physical and chemical properties to tailor the nanoparticle properties for high performances in the aforementioned biomedical applications.[20] Although size-dependent properties are well documented in spherical nanoparticles, investigations on shaped nanoparticles with different aspect ratios (i.e., different dimensional sizes) are still limited, especially on iron oxides. When varying the shape, the atomic arrangements in each facet of the nanocrystal can be altered, thus conferring new properties and applications. In particular, the anisotropic-shaped iron oxide nanoparticles (IONPs) with high aspect ratios have been shown to be strong MRI contrast agents, given the increased transverse relaxivity, r_2, due to the linear clustering effect[20] and more power hyperthermia agents.[21] Additionally, anisotropic magnetic nanoparticles with high aspect ratios exhibited higher magnetic moments, which yielded a higher separation efficiency when applied in magnetic separation and manipulation, even upon using a weaker magnetic field.[22] For the in vivo biomedical applications, such as imaging contrast agents or probes and drug-delivery systems, anisotropic nanocrystals in a certain range of aspect ratios exhibit favorable pharmacokinetics, with longer blood circulation time and tumor tissue uptake and retention compared to those of spherical nanoparticles.[23,24] Furthermore, nonspherical nanoparticles demonstrated the potential for multivalent and

selective biofunctionalization along with enhanced cell–particle interactions.[8,25,26] To take full advantage of their unique and improved physical and chemical attributes, robust and easy-to-scale synthetic methods that allow for rational control of the size, shape, and composition of nanostructures are necessary. Unlike varying the core size of spherical IONPs, which has been fairly well studied, deliberately controlling the iron oxide nanocrystal shape with different aspect ratios still remains very challenging.

In early attempts, several groups used platinum,[27,28] platinum–palladium,[29] cobalt,[30] or nickel[31] as a shape-control seed. However, with multiple metal components and additives, the particle growth mechanism and whether different reactants might work in competition or cooperation with one another are poorly understood. Moreover, the toxicity of these heavy metal contents in nanoparticles is a concern in future biological and clinical applications, especially in vivo applications. More recently, several different strategies for the synthesis of anisotropic pure metal nanocrystals have been reported. For example, long iron oxide nanorods (IONRs) with a length longer than 100 nm can be obtained by hydrothermal,[32] template-mediated,[33] microwave-assisted,[34] or precipitation methods.[35,36] When shorter nanorods are prepared, seed growth on the side facets of FeO nanocubes[31] or high-temperature thermal decompositions of β-FeOOH can also be applied.[37]

With an attempt to develop a robust synthesis procedure of IONRs and rationally control the morphological and physical properties of IONRs, herein, we present a versatile one-step solvothermal method for the preparation of IONRs with different aspect ratios (e.g., IONRs with lengths of 25 or 50 nm and mean diameters of 5 and 8 nm, respectively). Transmission electron microscopy (TEM), energy-dispersive X-ray spectroscopy (EDS), alternating gradient field magnetometry (AGM), and magnetic resonance relaxometry were used to characterize the physical properties of the resultant IONRs. To demonstrate potential biomedical applications, we prepared ligand-conjugated IONRs to examine the performance of biomarker specific detection and separation of metastatic pediatric brain tumor medulloblastoma cells in vitro. The higher r_2 values exhibited in IONRs compared to those in their spherical counterparts also render their potential as MRI contrast agents for molecular imaging applications.

2. EXPERIMENTAL SECTION

2.1. Chemicals and Materials.

Iron(III) acetylacetonate (Fe-(acac)$_3$), polyethyleneimine (PEI, 10 kDa, 50 wt %, aqueous solution), octyl(or phenyl)ether, and oleylamine were purchased from Fisher Chemicals (Fair Lawn, NJ). Holotransferrin (human), 3-(triethoxysilyl)propyl succinic anhydride (TSP), amine-terminated poly(ethylene glycol) (PEG), tetrahydrofuran (THF), fluorescein isothiocyanate (FITC), hexane, ethanol, and 3-(4,5-dimethylthiazol-2-yl)-2,5-diphenyltetrazolium bromide (MTT) assay kits were purchased from Sigma-Aldrich (St. Louis, MO). Sulfosuccinimidyl-4-(*N*-maleimidomethyl)cyclohexane-1-carboxylate (Sulfo-SMCC), Traut's reagent, *N*-(hydroxysulfosuccinimide) (Sulfo-NHS), 1-ethyl-3-[3-dimethylaminopropyl] carbodiimide hydrochloride (EDC), bicinchoninic acid (BCA) protein assay kit, streptomycin, and penicillin (10 000 U/mL penicillin, 10 000 μg/mL streptomycin in 0.85% saline) were purchased from Thermo Fisher Scientific (Waltham,

MA). CellTracker Green 5-chloromethylfluorescein diacetate, ProLong Gold anti-fade mountant with 4′,6-diamidino-2-phenylindole (DAPI), Vybrant Dil cell-labeling solution, and magnetic beads of 4.5 μm in diameter (Dynabeads M-450 Epoxy) were purchased from Life Technologies (Carlsbad, CA). Fetal bovine serum (FBS), Eagle's minimum essential medium, Dulbecco's modification of Eagle's medium, Roswell Park Memorial Institute 1640 (RPMI 1640) medium, and phosphate-buffered saline (PBS) were purchased from Corning (Corning, NJ). Cell media and supplements were acquired from Invitrogen. Milli-Q water (18.2 MΩ) was applied in all phases of the preparation. All chemicals were used without further purification.

2.2. Synthesis of IONRs and Spherical IONPs.

Each of the reactions was conducted under a N_2 atmosphere or argon atmosphere using the standard Schlenk line setup. The synthetic apparatus consists of the following elements: a Schlenk flask, a heating mantle with quartz wool insulation, and a thermocouple placed inside the flask. Analyzing the temperature inside the flask compared to that outside the flask showed very little temperature difference after adjusting for equilibrium in the flask (the internal thermocouple reads 195 °C when the external thermocouple reads 200 °C). To synthesize IONRs, $Fe(acac)_3$ (4 mmol) was mixed with PEI (2.5 or 1 mL), octyl(or phenyl)ether (10 mL), and oleylamine (2 mL, 6 mmol) and heated at 200 °C under argon protection for 4 h. To control the aspect ratio of the IONRs, two different concentrations of PEI (i.e., 50 wt %, aq. solution in 2.5 or 1 mL) were used. To synthesize other shapes of nanoparticles, the temperature, reaction time, and oleylamine concentration were varied and optimized. For instance, by changing the oleylamine concentration but keeping the other reaction parameters the same as those in the preparation of the 50 nm nanorods, nanoparticles with hexagonal and spherical shapes can be obtained. More specifically, a molar ratio of 1:7 (iron salt/oleylamine) gives a hexagon-like shape and a molar ratio of 1:8 gives 10 nm spherical nanoparticles. In the synthesis, oleylamine acts as a reducing agent and the reduction takes place when the mixture turns black. All of the resultant products were cooled to room temperature and purified through magnetic separation with an external permanent magnet using a process involving the isolation of the nanoparticles in a solution of hexane (2 mL) and ethanol (30–40 mL). This entire separation procedure was repeated several times.

For the synthesis of spherical IONPs that can be used for comparison with IONRs, we used a general thermal decomposition approach of $Fe(acac)_3$ in a solvent mixture of phenyl ether, oleylamine, and low amounts of PEI. The reaction uses a high temperature of 250 °C. $Fe(acac)_3$ (3 mmol) was reacted with phenyl ether (30 mL), oleylamine (9 mmol), and 0.1 mL PEI under nitrogen. The mixture was refluxed for 30 min. This reaction gives IONPs with a core size of 5 nm. Furthermore, to increase the nanoparticle size to 25 and 50 nm, seed-mediated synthesis was used. Using 10 mg of seeds mixed with 5 mmol of $Fe(acac)_3$, 10 mmol of stearyl alcohol, and 4 mmol of oleylamine led to IONPs with a core size of 25 nm, whereas changing the mass of the seeds to 0.1 mg but keeping the other conditions the same resulted in IONPs with a core size of 50 nm.

2.3. Coating and Stabilizing IONRs and IONPs with PEG.

PEG-NH_2 was used to functionalize IONR surfaces following a modified procedure by Fang et al.[38] First, IONRs were silanized using TSP by reacting for 12 h at 105 °C under an argon atmosphere. They were then collected using magnetic separation and washed with 50 mL hexane several times. The precipitated IONRs then were dissolved in THF (7 mL), PEG with amine terminal groups (170 mg, MW: 2 kDa) was added to the IONRs, and the mixture was sonicated at 50 °C for about 20 h. Finally, the PEG-coated IONRs (IONR-PEG-NH_2) were, once again, purified using magnetic separation and washed with excess hexane. The same coating procedure was applied to the spherical IONPs, which were prepared as controls to determine the shape-specific properties.

2.4. Functionalization of PEG-Coated IONRs and IONPs with Targeting Ligands.

A solution of 2 mg/mL IONR-PEG-NH_2 in PBS was reacted for 1 h with a Sulfo-SMCC linker (at a concentration of 2 mg/mL). The resulting compounds, Sulfo-SMCC-IONRs, were then purified using a PD-10 column to remove the free linkers and free nanoparticles. Additionally, the transferrin receptor (TfR) targeted ligand holotransferrin (Tf), conjugated with the FITC, was thiolated via a thiolation reaction by mixing it overnight with Traut's reagent (in a molar ratio of 1:15). The thiolation reaction was performed in pH 8.5 borate buffer (0.1 M). The resulting product was then purified using a desalting spin column. Sulfo-SMCC-IONRs were then incubated with thiolated-Tf in PBS for 4 h at room temperature. Tf-IONRs were purified, using both differential centrifugation and magnetic separation. The number of Tf ligands conjugated to the IONR surface was determined by a BCA protein assay.[39] The iron concentrations of different samples were determined by the colorimetric method used in our previous work.[39]

To demonstrate the targeting ability of Tf-IONRs, we prepared a control sample, that is, nontargeting ligand bovine serum albumin (BSA)-conjugated IONRs (BSA-IONRs), using a procedure similar to that used for conjugating IONRs with Tf. BSA was also labeled with FITC before being conjugated onto IONRs. The same conjugation procedure was applied for spherical IONPs to obtain Tf-IONPs and BSA-IONPs.

2.5. Characterizations of IONPs and IONRs.

Both the size and morphology of the synthesized IONRs and spherical IONPs were examined using a TEM (HitachiH-7500), with an accelerating voltage of 75 kV. The samples were prepared by dropping a diluted amount of nanoparticles onto the TEM grid. The size and dimensions of the prepared IONPs and IONRs were determined by averaging measurements from 50 randomly selected particles in the field of view of a TEM image. The magnetic moment versus applied magnetic field (M–H) curves of the magnetic nanoparticles were recorded using a Princeton AGM at room temperature.

X-ray diffraction (XRD) measurements were performed using a Philips X′Pert-Diffractometer with (Bragg-Brentano-geometry, Cu Kα-rays, $U = 45$ kV; $I = 40$ mA). Statistical analyses for mean values, standard deviations, and Student's t-test were performed using Microsoft Office Excel software (Microsoft Corporation, Redmond, WA). To study the MRI contrast enhancement properties of prepared nanorods and spherical

nanoparticles, the transverse relaxation time (T_2) and relaxivity (r_2) were measured by an MR scanner at the field strength of 3 T (Siemens 3T Tim/Trio; Siemens Healthcare, Erlangen, Germany). A set of MRI phantom tubes containing solutions of IONRs and IONPs (2 mL) with different iron concentrations (0.008–0.125 mM) was scanned in the MRI scanner. Images were recorded using a multiecho spin echo (SE) sequence performed with a time of repeat of 2520 ms and an array of 20 different time of echo points, starting at 12.2 ms, with an increment of 12.2 ms. A plugin program in the software ImageJ (NIH) was used to calculate the mean values of the signal intensities of the regions of interest, and the T_2 values of each sample was calculated by exponentially fitting MRI signal intensities. Finally, the linear correlation slope between the relaxation rates ($1/T_2$) at different iron concentrations was used to determine the transverse relaxivity, r_2, as reported by us earlier.[40]

2.6. Targeting and Specific Cell Binding of Tf-IONRs to TfR Overexpressed Cells.

The pediatric brain tumor medulloblastoma D556 cell line with TfR highly overexpressed was used for testing the specificity of the targeted IONRs or IONPs, functionalized with Tf as the targeting ligand to TfR. The cells were treated with 0.2 mg/mL FITC-labeled Tf-IONRs or Tf-IONPs at 37 °C for 3 h. Briefly, the cells were cultured under 37 °C under humidified conditions (5% CO_2). FBS (10%) with 1% penicillin–streptomycin was supplemented in the cell media. The cells (5×10^5) were seeded in each well of eight-well-chambered slides. After 36 h of incubation, the medium was replaced and the nanoparticles (0.1 mg/mL) were added into the cell medium and further incubated for 3 h at 37 °C. The cell medium was then discharged, and the collected cells were washed with PBS three times. The cell binding or internalization of the targeted nanoparticles was observed using a fluorescent microscope (Zeiss Axioplan 2, Thornwood, NY) at 488 nm excitation and 515 nm emission.[41] We performed the same experiments using nonspecific.

2.7. Magnetic Separation of Cancer Cells.

Because immune-magnetic cell separation is one of the most adopted biomedical applications of magnetic particles, to demonstrate whether shaped IONRs show improved performance in biomarker-targeted applications or not, we performed immunomagnetic cell separation experiments using developed Tf-IONRs, with spherical Tf-IONPs and commercially available magnetic Dynabeads, widely used in research laboratories, as a comparison. The cell separation experiments were performed using a procedure reported recently.[42] Briefly, 2.0×10^4 D556 cells per well were prepared and grown for 24 h prior to separation. After removal of the culture medium, D556 cells were incubated with a 0.2 mg/mL concentration of nanoparticles (IONRs; spherical IONPs; and commercially available magnetic Dynabeads M-270 Epoxy) in fresh medium for 1 h at 4 °C. Subsequently, the medium solution was removed and PBS was used to wash cells three times. Next, the cells were detached and placed into tubes and diluted in 1 mL of PBS. The tube containing cell suspensions was then inserted into a permanent magnet (Fisher, Cat. No.: CS15000) for a selected time, for example, 2.5 or 5 min. The cells attached with magnetic nanoparticles were separated from the suspension. The captured D556 cells were resuspended in PBS and were counted using a hemocytometer. Separately, the prestained D556 cells were transferred onto the PLL-coated slide, fixed with 4% paraformaldehyde in PBS, and then mounted with the Prolong Gold anti-fade mounting reagent containing DAPI. The cells were observed

under the fluorescence microscope (Olympus BX41; Olympus, Center Valley, PA). Various time points were used to test and measure the cell capture performances of different shapes of magnetic materials (i.e., IONRs), IONPs, and commercially available magnetic beads (Dynabeads M-270 Epoxy).

2.8. In Vitro Cytotoxicity Analysis.

The cytotoxicity of the reported IONRs was examined using the MTT assay, Hela cells, and D556 medulloblastoma cells using the protocol reported in our earlier study.[43] Briefly, 1×10^4 Hela cells or D556 cells per well of a 96-well plate were seeded with IONRs at selected concentrations for 24 h. The IONR-treated cells were then washed with PBS three times. Subsequently, the MTT solution (100 μL per well) was added into the cells. The resulting mixture was incubated for 4 h, followed by 5 min of pipetting with DMSO (100 μL/well). The absorbance at 570 nm was read using a plate reader. The untreated cells were considered to have 100% viability. Comparisons of cell viability between the IONR-treated groups and controls were performed using one-way analysis of variance and the Student *t*-test (unpaired, two tails).

3. RESULTS AND DISCUSSION

3.1. Shape-Controlled Synthesis of IONRs with Different Aspect Ratios.

With a one-pot synthesis, IONRs that are 25 and 50 nm in length and 5 and 8 nm in diameter (aspect ratios of 5 and 6.3) can be readily obtained. After coating with PEG, they were single dispersed into the various solvents and biofunctionalized. The prepared IONRs are highly stable in biological media and possess highly magnetic properties. The synthetic procedure involves the reaction of iron acetylacetonate with PEI in the presence of oleylamine and phenyl ether, followed by the solvothermal method at 200 °C under an inert gas atmosphere. The method reported here allows the preparation of short and thin nanorods, long and thick nanorods, and even longer and thinner nanowires by just varying the PEI concentrations. This robust synthesis procedure can be applied for a scale-up production without a size selection of products. The morphologies of the resultant IONRs are presented in Figure 1. Statistical analysis (Figure S1) indicated mean lengths of 25.4 ± 1.9 and 50 ± 3.2 nm for the reported 25 and 50 nm (in length) IONRs, respectively. To provide examples for this report, we only show nanorods with a mean length of 25 nm and a mean diameter of 5 nm (Figure 1A), resulting from the use of 2.5 mL of PEI, and those with a length of 50 nm and a mean diameter of 5 nm, resulting from the use of 1 mL of PEI (Figure 1B).

High-resolution TEM images show that IONRs tend to align parallel to each other along their long axes. Elongated 50 nm nanorods are parallel to the set of (111) planes, indicated by observation of the fringe spacing of 0.203 nm (Figure 1C). Through the previously attached TSP linker, PEG-NH_2 was then introduced onto IONR surfaces successfully. EDS measurements, as shown in Figure 1D, reveal the composition of the nanorods having a core of iron oxide and a coating shell of silane, which is evidenced by a sharply increased silicon (Si) peak after the functionalization steps. Notably, the copper peak is attributed to the TEM copper grid. To further study the crystal structure of the synthesized oleylamine-coated nanorods, XRD measurements were conducted on 50 nm IONRs. The sample was collected

as a thin film on a glass side by drying chloroform-dissolved IONRs in an oven. As shown in Figure 1E, the inverse spinel structure of IONRs was easily observed, although the typical broadening peaks were presented as expected, which is due to the effect of small crystallite domain size. The position of the peaks is in good agreement with the XRD reference pattern (shown as the bottom columns in Figure 1E), which demonstrated that the crystalline phase of the prepared IONRs is magnetite instead of other phases of iron oxide.

Considering the formation mechanism of the rodlike anisotropic nanoparticles, PEI concentration, reaction time, reaction temperature, and oleylamine concentration are among the factors affecting their elongation during growth. As examples, Figure 2A,B shows a set of TEM images of different shapes of nanoparticles obtained at different reaction temperatures (top panel) and oleylamine concentrations (lower panel). Thus, keeping the same reaction condition used for the formation of 50 nm IONRs, but changing the temperature to 230 °C (Figure 2A) and 250 °C (Figure 2B), the rod shape was disrupted, leading to nanoparticles that were less uniform in shape and size. Our experience suggests that under these reaction conditions at higher temperatures both the nucleation and growth rate increased and therefore nonuniform nanorods and spherical nanoparticles were formed. Moreover, we observed that the reaction time greatly affected the final shape of the nanoparticles. When the reaction was maintained for 4 h after reduction, hollowed nanorods may be present (Figure 2C). Of note, for the formation of the uniform rods, the reaction was stopped immediately after reduction (the reduction occurs when the mixture turns black).

Additionally, increasing the oleylamine concentration from a molar ratio of iron salt/oleylamine may cause shape change from nanorod to hexagon-like or spherelike. For example, a molar ratio of 1:7 gives a hexagon-like shape (Figure 2D), a molar ratio of 1:8 gives 10 nm spheres (Figure 2E), and a molar ratio of 1:9 gives ultrasmall 3.5 nm spherical nanoparticles (Figure 2F). Finally, to promote the formation of super-paramagnetic IONRs, it is essential to carry out the synthesis in a N_2 atmosphere.

To make IONRs stable in hydrophilic media, the IONR surface was coated with a layer of PEG-NH_2, following a modified protocol reported by Fang et al.[38] To further evaluate the stability of IONRs, the hydrodynamic size change of IONRs was monitored in various solutions, such as aqueous NaCl solution, PBS, and 100% FBS at a concentration of 0.2 mg/mL for a period of 1, 2, 4, 8, 12, and 24 h, respectively. The PEG-NH_2 coated IONRs (with a length of 50 nm by TEM measurement) remain single dispersed, with hydrodynamic sizes only slightly increased from 77.5 to 85.2 nm within 24 h, demonstrating good stability in aqueous media and against the nonspecific protein absorption in 100% FBS.

3.2. Stronger Magnetic Properties with IONRs.

We examined the magnetic properties of the IONRs of different aspect ratios and IONPs by measuring the magnetic moment versus applied magnetic field (*M*–*H*) curves using an AGM at room temperature. The *M*–*H* curves of IONRs with different aspect ratios shown in Figure 3 revealed that these IONRs are superparamagnetic. With an increase in the nanorod length to 50 nm, the magnetization saturation value increases to 75 emu g^{-1}. The lower magnetization value of the smaller IONRs was attributed to the increased surface spin disorder layer. Further, the MS values of spherical IONPs are even lower compared to those

of the IONRs: 1.8 emu g^{-1} for spherical IONPs and from 8 emu g^{-1} (25 nm) to 75 emu g^{-1} (50 nm) for IONRs, as shown in Figure 3A–C.

Given the high magnetization values, these IONRs are expected to have a strong contrast-enhancing effect in the MRI. In Figure 4, T_2-weighted MR images of IONRs with different iron concentrations recorded at a field strength of 3 T are presented. Significant iron concentration-dependent signal attenuation induced by IONRs was observed when increasing the Fe concentrations from 0.001 to 0.089 mM (Figure 4).

The transverse relaxivity, r_2, for IONRs with lengths of 25 and 50 nm are 670.57 and 905.53 mM^{-1} s^{-1}, respectively. The observation of an increased r_2 value from longer IONRs is consistent with the earlier report by Mohapatra et al.[44] and is possibly related to their high magnetization saturation value and relatively large surface area. In comparison, the r_2 values of spherical IONPs with diameters of 25 and 50 nm increase from 326.2 to 523.3 mM^{-1} s^{-1}, respectively. Hence, IONRs exhibit superior T_2-weighted contrast properties that can potentially improve the sensitivity of MRI detection. In addition to the potential improvement of pharmacokinetics and tissue penetration and retention with nonspherical anisotropic shape, the advantages of high relaxivity MRI contrast agents, particularly in nanoparticles, which generally have low delivery efficiency to the targeted tissue (e.g., a tumor) and high nonspecific uptake and low degradation in the liver, include reducing the dosage, thus minimizing potential toxicity risks, improving the sensitivity for molecular-targeted imaging when the levels of targeted biomarkers are intrinsically limited and detecting small lesions when only a small amount of the contrast agent can reach and accumulate.

3.3. Functionalized IONRs for Biomarker Targeting.

The capability of biomarker targeting of these IONRs was tested on TfR overexpressed medulloblastoma cells, which is the most common brain cancer in children. Medulloblastoma cancer cells were incubated with either IONRs or spherical IONPs conjugated with TfR-targeted Tf ligands or inactive nontargeted BSA-labeled FITC. In addition, blocking experiments in which the TfR of cells were pretreated with a fixed amount of Tf to block the TfRs were performed to further confirm the binding specificity of Tf-IONRs to TfRs. Using fluorescence imaging (Figure 5A–C), we can compare the amount of cells captured by the various nanoparticles. The results show that the anisotropic properties of the IONRs confer superiority in targeting biomarker-overexpressed cells compared with spherical IONPs (Figure 5D–F). Fluorescence images of TfR-overexpressing medulloblastoma D556 cells treated with different nanoparticle conjugates, shown in Figure 5A–F, reveal that the green fluorescence from FITC is stronger in cells treated with Tf-conjugated IONRs (Figure 5A) or IONPs (Figure 5D) compared to that in the cells treated with spherical BSA-conjugated IONRs (Figure 5B) and IONPs (Figure 5E). The blocking of TfRs reduced the cellular uptake of targeted Tf-IONPs (Figure 5C) and Tf-IONRs (Figure 5F).

Although the spherical nanoparticles were found to be effective for cell targeting, the anisotropic IONRs exhibit a superb capability of targeting cancer cells. The superior targeting capability of the nanorods compared to that of the spherical nanoparticles is

demonstrated by the observed stronger green florescence intensity (Figure 5A), which is much higher than that of the spherical nanoparticle cells (Figure 5D). Furthermore, cytotoxicity experiments from the MTT assay using Hela cells and D556 medulloblastoma cells (Figure S2) revealed that the cell viabilities of both Hela and D556 cells still reached 83% when surface-coated IONRs were added at very high concentrations of 0.50 Fe mg/mL; however, at lower concentrations (<0.13 Fe mg/mL), coated IONRs did not exhibit statistically significant cytotoxicity to Hela cells ($p \geq 0.05$).

3.4. More Efficient Immunomagnetic Cell Separation with IONRs.

To further demonstrate the utility of the reported IONRs in biological applications, in particular, using Tf-IONRs to capture cancer cells in the medium, the performance of Tf-IONRs in capturing D556 cancer cells in the 1 mL medium was compared to that of their spherical IONPs in mimic of immunomagnetic cell capturing and separation applications commonly used in biomedical laboratories.

Tf functionalized IONRs, with a length of 50 nm and diameter of 5 nm, were investigated for magnetic separation of transferrin-overexpressed medulloblastoma D556 cells, which have a high tendency of metastasis through the cerebral spinal fluid (CSF). The performance or efficiency of detecting and separating cancer cells was compared to that of commercial spherical IONPs or macron-sized magnetic beads (i.e., Dynabeads) widely used for cell separation experiments. On the basis of the substantial magnetization difference, we expect the IONRs to provide a more efficient separation in a shorter time window. The experiments were performed under the same conditions (i.e., the same Fe concentration, medium, temperature, incubation time, and permanent magnet) but with varying nanoparticles, nanorods, or Dynabeads and lengths of separation time. The fluorescent images of the medulloblastoma cancer cells captured by different nanoparticles or nanorods as well as Dynabeads using a magnetic separation time of 2.5 min are shown in Figure 6.

We used the amount of captured cells to estimate the efficiency of the cell capture and separation given a 5 min magnetic separation time and 0.2 mg Fe/mL of nanomaterial used. The results showed that the percentages of cells captured were 98 ± 3.2% for IONRs compared to 78.67 ± 5.3% for spherical IONPs and 40 ± 3.2% for Dynabeads ($n = 3$, $p < 0.05$). When changing separation time to 2.5 min, the amounts of cells captured were reduced, being 92 ± 3.2% for IONRs compared to 37.33 ± 5.3% for spherical IONPs and 14 ± 3.2% for Dynabeads ($n = 3$, $p < 0.05$, at 0.2 mg/mL Fe). For these two treatments, the separation efficiency was higher when using the IONRs. For instance, for a 2.5 min experiment time, the separation yield was higher by a factor of approximately 6.5 for the nanorods when compared to that of the Dynabeads (92 ± 3% vs 14 ± 2%) and by a factor of 2.4 (92 ± 3% vs 37 ± 2%) when compared to that of the spherical IONPs prepared under similar conditions.

Xu et al.[45] have previously developed spherical IONPs and applied them in the immunomagnetic separation of tumor cells. The cell-separation process involved the use of polymer-coated spherical IONPs with a core size of 30 nm, which were conjugated with antihuman epithelial growth factor receptor 2 (anti-HER2 or anti-HER2/neu) antibodies. In that work, after 10 min of incubation with spherical IONPs at room temperature, 73.6% of

SK-BR3 cells spiked in 1 mL of fresh human whole blood were separated by the IONPs in 10 min. Using the nanorods reported in this work, we were able to isolate 98% of the cells in 5 min under similar conditions (e.g., the magnet, temperature, and volume of the media that cancer cells were spiked in). Others have also reported the performances of spherical IONPs[46,47] or beads[48] in cell separation and detection of various diseases.[49] In comparison, anisotropic IONRs reported in this work exhibited better performance than spherical IONPs or microsized magnetic beads. This is possibly attributed to their high surface ratio and high magnetic moments. Further studies need to be conducted to compare and analyze the efficiency of the nanorods and spherical particles in cell detection and separation using more biological application-relevant media, such as whole blood or CSF samples.

4. CONCLUSIONS

We presented a one-step oleylamine-mediated procedure that was used to successfully synthesize IONRs with lengths ranging from 25 to 50 nm and diameters from 5 to 8 nm. As compared to conventional spherical IONPs, IONRs at a similar material volume and mass provide stronger magnetic properties, including magnetic saturation and relaxation times, compared to spherical IONPs. Additionally, we showed, as an example for potential biomedical application, that the reported anisotropic IONRs offer an improved performance in biomarker-targeted cell capture and separation and therefore can be used for cancer detection and diagnosis. It is anticipated that future development of such anisotropic IONPs and systematic investigations of the functional properties and biological behaviors will lead to a range of new or improved biomedical applications in in vivo MRI, molecular imaging, drug delivery, as well as in vitro magnetic device-based detection.

Supplementary Material

Refer to Web version on PubMed Central for supplementary material.

ACKNOWLEDGMENTS

This work is supported in part by a grant (R01CA154846-02) from NIH, NCI's Cancer Nanotechnology Platform Project (CNPP) grant (U01CA151810-02), and a seed grant from the Center for Pediatric Nanomedicine of Children's Healthcare of Atlanta. The authors thank Steve Larson of the Department of Physics and Astronomy at the University of Georgia for their assistance in recording XRD data.

REFERENCES

(1). Gobbo OL; Sjaastad K; Radomski MW; Volkov Y; Prina-Mello A Magnetic Nanoparticles in Cancer Theranostics. Theranostics 2015, 5, 1249–1263. [PubMed: 26379790]

(2). Huang J; Wang L; Zhong X; Li Y; Yang L; Mao H Facile Non-hydrothermal Synthesis of Oligosaccharide Coated Sub-5 nm Magnetic Iron Oxide Nanoparticles with Dual MRI Contrast Enhancement Effects. J. Mater. Chem. B 2014, 2, 5344–5351.

(3). Li Y; Li CH; Talham DR One-step Synthesis of Gradient Gadolinium Ironhexacyanoferrate Nanoparticles: a New Particle Design Easily Combining MRI Contrast and Photothermal Therapy. Nanoscale 2015, 7, 5209–5216. [PubMed: 25706057]

(4). Khafaji M; Vossoughi M; Hormozi-Nezhad MR; Dinarvand R; Borrnert F; Irajizad A A New Bifunctional Hybrid Nanostructure as an Active Platform for Photothermal Therapy and MR Imaging. Sci. Rep 2016, 6, No. 27847. [PubMed: 27297588]

(5). Bakhtiary Z; Saei AA; Hajipour MJ; Raoufi M; Vermesh O; Mahmoudi M Targeted Superparamagnetic Iron Oxide Nanoparticles for Early Detection of Cancer: Possibilities and Challenges. Nanomedicine 2016, 12, 287–307. [PubMed: 26707817]

(6). Shi C; Thum C; Zhang Q; Tu W; Pelaz B; Parak WJ; Zhang Y; Schneider M Inhibition of the Cancer-Associated TASK 3 Channels by Magnetically Induced Thermal Release of Tetrandrine from a Polymeric Drug Carrier. J. Controlled Release 2016, 237, 50–60.

(7). Liu Y; Cui T; Wu T; Li Y; Tong G Excellent Microwave-absorbing Properties of Elliptical Fe_3O_4 Nanorings Made by a Rapid Microwave-Assisted Hydrothermal Approach. Nanotechnology 2016, 27, No. 165707. [PubMed: 26962718]

(8). Das R; Alonso J; Nemati Porshokouh Z; Kalappattil V; Torres D; Phan MH; Garaio E; García JÁ; Sanchez Llamazares JL; Srikanth H Tunable High Aspect Ratio Iron Oxide Nanorods for Enhanced Hyperthermia. J. Phys. Chem. C 2016, 120, 10086–10093.

(9). Nadeem M; Ahmad M; Akhtar MS; Shaari A; Riaz S; Naseem S; Masood M; Saeed MA Magnetic Properties of Polyvinyl Alcohol and Doxorubicine Loaded Iron Oxide Nanoparticles for Anticancer Drug Delivery Applications. PLoS One 2016, 11, No. e0158084. [PubMed: 27348436]

(10). Park J; Kadasala NR; Abouelmagd SA; Castanares MA; Collins DS; Wei A; Yeo Y Polymer-Iron Oxide Composite Nanoparticles for EPR-independent drug delivery. Biomaterials 2016, 101, 285–295. [PubMed: 27310916]

(11). Tang Z; Zhang L; Wang Y; Li D; Zhong Z; Zhou S Redox-responsive Star-Shaped Magnetic Micelles with Active-Targeted and Magnetic-guided Functions for Cancer Therapy. Acta Biomater. 2016, 42, 232–246. [PubMed: 27373437]

(12). Xiong D; Wang X; Li W; Liu L Facile Synthesis of Iron Phosphide Nanorods for Efficient and Durable Electrochemical Oxygen Evolution. Chem. Commun 2016, 52, 8711–8714.

(13). Khan S; Rizvi SM; Ahmad V; Baig MH; Kamal MA; Ahmad S; Rai M; Zafar Iqbal AN; Mushtaq G; Khan MS Magnetic Nanoparticles: Properties, Synthesis and Biomedical Applications. Curr. Drug Metab 2015, 16, 685–704. [PubMed: 26264204]

(14). Haham H; Natan M; Gutman O; Kolitz-Domb M; Banin E; Margel S Engineering of Superparamagnetic Core–Shell Iron Oxide/N-Chloramine Nanoparticles for Water Purificatio. ACS Appl. Mater. Interfaces 2016, 8, 18488–18495. [PubMed: 27348740]

(15). Liu J; Xia T; Wang S; Yang G; Dong B; Wang C; Ma Q; Sun Y; Wang R Oriented-Assembly of Hollow FePt Nanochains with Tunable Catalytic and Magnetic Properties. Nanoscale 2016, 8, 11432–11440. [PubMed: 26971675]

(16). Jia CJ; Sun LD; Luo F; Han XD; Heyderman LJ; Yan ZG; Yan CH; Zheng K; Zhang Z; Takano M; Hayashi N; Eltschka M; Klaui M; Rudiger U; Kasama T; Cervera-Gontard L; Dunin-Borkowski RE; Tzvetkov G; Raabe J Large-Scale Synthesis of Single-Crystalline Iron Oxide Magnetic Nanorings. J. Am. Chem. Soc 2008, 130, 16968–16977. [PubMed: 19053430]

(17). Milosevic I; Motte L; Aoun B; Li T; Ren Y; Sun C; Saboungi ML Effects of Coating Spherical Iron Oxide Nanoparticles. Biochim. Biophys. Acta 2017, 1861, 3621–3626.

(18). Savla R; Minko T Nanoparticle Design Considerations for Molecular Imaging of Apoptosis: Diagnostic, Prognostic, and Therapeutic Value. Adv. Drug Delivery Rev 2016, S0169–409X, 30209–30215.

(19). Kwizera EA; Chaffin E; Shen X; Chen J; Zou Q; Wu Z; Gai Z; Bhana S; O'Connor R; Wang L; Adhikari H; Mishra SR; Wang Y; Huang X Size- and Shape-Controlled Synthesis and Properties of Magnetic-Plasmonic Core-Shell Nanoparticles. J. Phys. Chem. C 2016, 120, 10530–10546.

(20). Kolhatkar AG; Jamison AC; Litvinov D; Willson RC; Lee TR Tuning the Magnetic Properties of Nanoparticles. Int. J. Mol. Sci 2013, 14, 15977–16009. [PubMed: 23912237]

(21). Sun M; Xu L; Ma W; Wu X; Kuang H; Wang L; Xu C Hierarchical Plasmonic Nanorods and Upconversion Core-Satellite Nanoassemblies for Multimodal Imaging-Guided Combination Photo-therapy. Adv. Mater 2016, 28, 898–904. [PubMed: 26635317]

(22). Son SJ; Reichel J; He B; Schuchman M; Lee SB Magnetic Nanotubes for Magnetic-Field-Assisted Bioseparation, Biointeraction, and Drug Delivery. J. Am. Chem. Soc 2005, 127, 7316–7317. [PubMed: 15898772]

(23). Shukla S; Eber FJ; Nagarajan AS; DiFranco NA; Schmidt N; Wen AM; Eiben S; Twyman RM; Wege C; Steinmetz NF The Impact of Aspect Ratio on the Biodistribution and Tumor Homing of Rigid Soft-Matter Nanorods. Adv. Healthcare Mater 2015, 4, 874–82.

(24). Agarwal R; Jurney P; Raythatha M; Singh V; Sreenivasan SV; Shi L; Roy K Effect of Shape, Size, and Aspect Ratio on Nanoparticle Penetration and Distribution Inside Solid Tissues Using 3D Spheroid Models. Adv. Healthcare Mater 2015, 4, 2269–80.

(25). Lankveld DP; Rayavarapu RG; Krystek P; Oomen AG; Verharen HW; van Leeuwen TG; De Jong WH; Manohar S Blood Clearance and Tissue Distribution of PEGylated and Non-PEGylated Gold Nanorods after Intravenous Administration in Rats. Nanomedicine 2011, 6, 339–349. [PubMed: 21385136]

(26). Kolhar P; Anselmo AC; Gupta V; Pant K; Prabhakarpandian B; Ruoslahti E; Mitragotri S Using Shape Effects to Target Antibody-Coated Nanoparticles to Lung and Brain Endothelium. Proc. Natl. Acad. Sci. U.S.A 2013, 110, 10753–10758. [PubMed: 23754411]

(27). Sahu NK; Prakash A; Bahadur D Role of Different Platinum Precursors on the Formation and Reaction Mechanism of FePt Nanoparticles and their Electrocatalytic Performance Towards Methanol Oxidation. Dalton Trans. 2014, 43, 4892–4900. [PubMed: 24492706]

(28). Chou SW; Liu CL; Liu TM; Shen YF; Kuo LC; Wu CH; Hsieh TY; Wu PC; Tsai MR; Yang CC; Chang KY; Lu MH; Li PC; Chen SP; Wang YH; Lu CW; Chen YA; Huang CC; Wang CR; Hsiao JK; Li ML; Chou PT Infrared-Active Quadruple Contrast FePt Nanoparticles for Multiple Scale Molecular Imaging. Biomaterials 2016, 85, 54–64. [PubMed: 26854391]

(29). Guo S; Zhang S; Sun X; Sun S Synthesis of Ultrathin FePtPd Nanowires and Their Use as Catalysts for Methanol Oxidation Reaction. J. Am. Chem. Soc 2011, 133, 15354–15357. [PubMed: 21894999]

(30). Mendoza-Garcia A; Zhu H; Yu Y; Li Q; Zhou L; Su D; Kramer MJ; Sun S Controlled Anisotropic Growth of Co-Fe-P from Co-Fe-O Nanoparticles. Angew. Chem., Int. Ed. Engl 2015, 54, 9642–9645. [PubMed: 26118355]

(31). Singh B; Ho CL; Tseng YC; Lo CT Controlled Synthesis and Magnetic Properties of Nickel Phosphide and Bimetallic Iron–Nickel Phosphide Nanorods. J. Nanopart. Res 2012, 14, 706.

(32). Khalil M; Yu J; Liu N; Lee RL Hydrothermal Synthesis, Characterization, and Growth Mechanism of Hematite Nanoparticles. J. Nanopart. Res 2014, 16, 2362.

(33). Kloust H; Zierold R; Merkl JP; Schmidtke C; Feld A; Pöselt E; Kornowski A; Nielsch K; Weller H Synthesis of Iron Oxide Nanorods Using a Template Mediated Approach. Chem. Mater 2015, 27, 4914–4917.

(34). Sayed FN; Polshettiwar V Facile and Sustainable Synthesis of Shaped Iron Oxide Nanoparticles: Effect of Iron Precursor Salts on the Shapes of Iron Oxides. Sci. Rep 2015, 5, No. 9733. [PubMed: 25939969]

(35). Narayanan S; Vijayal JJ; Adinaveen T; Bououdina M; Kennedy LJ Synthesis of α-Fe_2O_3 Sphere/Rod-Like Nanostructure via Simple Surfactant-Free Precipitation Route: Optical Properties and Formation Mechanism. J. Nanosci. Nanotechnol 2015, 15, 4558–4566. [PubMed: 26369080]

(36). Zhao YM; Li YH; Ma RZ; Roe MJ; McCartney DG; Zhu YQ Growth and Characterization of Iron Oxide Nanorods/Nanobelts Prepared by a Simple Iron-Water Reaction. Small 2006, 2, 422–427. [PubMed: 17193062]

(37). Wenlu L; Seung Soo L; Jiewei W; Carl HH; John DF Shape and Size Controlled Synthesis of Uniform Iron Oxide Nanocrystals through New Non-hydrolytic Routes. Nanotechnology 2016, 27, No. 324002. [PubMed: 27354334]

(38). Fang C; Bhattarai N; Sun C; Zhang M Functionalized Nanoparticles with Long-Term Stability in Biological Media. Small 2009, 5, 1637–1641. [PubMed: 19334014]

(39). Chen H; Wang L; Yeh J; Wu X; Cao Z; Wang YA; Zhang M; Yang L; Mao H Reducing Non-Specific Binding and Uptake Of Nanoparticles and Improving Cell Targeting with an Antifouling PEO-b-PγMPS Copolymer Coating. Biomaterials 2010, 31, 5397–407. [PubMed: 20398933]

(40). Zhang L; Zhong X; Wang L; Chen H; Wang YA; Yeh J; Yang L; Mao H T_1-Weighted Ultrashort Echo Time Method for Positive Contrast Imaging of Magnetic Nanoparticles and Cancer Cells Bound with the Targeted Nanoparticles. J. Magn. Reson. Imaging 2011, 33, 194–202. [PubMed: 21182139]

(41). Christian GD Analytical Chemistry, 5th ed.; John Wiley and Sons, Inc.: New York, 1994; pp 23–724.

(42). Lin R; Li Y; MacDonald T; Wu H; Provenzale J; Peng X; Huang J; Wang L; Wang AY; Yang J; Mao H Improving Sensitivity and Specificity of Capturing and Detecting Targeted Cancer Cells with Anti-Biofouling Polymer Coated Magnetic Iron Oxide Nanoparticles. Colloids Surf., B 2017, 150, 261–270.

(43). Li Y; Lin R; Wang L; Huang J; Wu H; Cheng G; Zhou Z; MacDonald T; Yang L; Mao H PEG-*b*-AGE Polymer Coated Magnetic Nanoparticle Probes with Facile Functionalization and Antifouling Properties for Reducing Non-specific Uptake and Improving Biomarker Targeting. J. Mater. Chem. B 2015, 3, 3591–3603. [PubMed: 26594360]

(44). Mohapatra J; Mitra A; Tyagi H; Bahadu r. D.; Aslam M Iron Oxide Nanorods as High-Performance Magnetic Resonance Imaging Contrast Agents. Nanoscale 2015, 7, 9174–84. [PubMed: 25849780]

(45). Xu H; Aguilar ZP; Yang L; Kuang M; Duan H; Xiong Y; Wei H; Wang A Antibody Conjugated Magnetic Iron Oxide Nanoparticles for Cancer Cell Separation in Fresh Whole Blood. Biomaterials 2011, 32, 9758–9765. [PubMed: 21920599]

(46). Bhana S; Wang Y; Huang X Nanotechnology for Enrichment and Detection of Circulating Tumor Cells. Nanomedicine 2015, 10, 1973–1990. [PubMed: 26139129]

(47). Wang C; Ye M; Cheng L; Li R; Zhu W; Shi Z; Fan C; He J; Liu J; Liu Z Simultaneous Isolation and Detection of Circulating Tumor Cells with a Microfluidic Silicon-Nanowire-Array Integrated with Magnetic Upconversion Nanoprobes. Biomaterials 2015, 54, 55–62. [PubMed: 25907039]

(48). Yang S; Yin S; Shang Y; Wang D; Ma W; He J; Guo J; Cai J; Liu X Specific Detection of Doot-and-Mouth Disease Serotype Asia 1 Virus by Carboxyl-Magnetic Beads Conjugated with Single-Domain Antibody. BMC Biotechnol. 2015, 15, 83. [PubMed: 26369792]

(49). Lin M; Chen JF; Lu YT; Zhang Y; Song J; Hou S; Ke Z; Tseng HR Nanostructure Embedded Microchips for Detection, Isolation, and Characterization of Circulating Tumor Cells. Acc. Chem. Res 2014, 47, 2941–2950. [PubMed: 25111636]

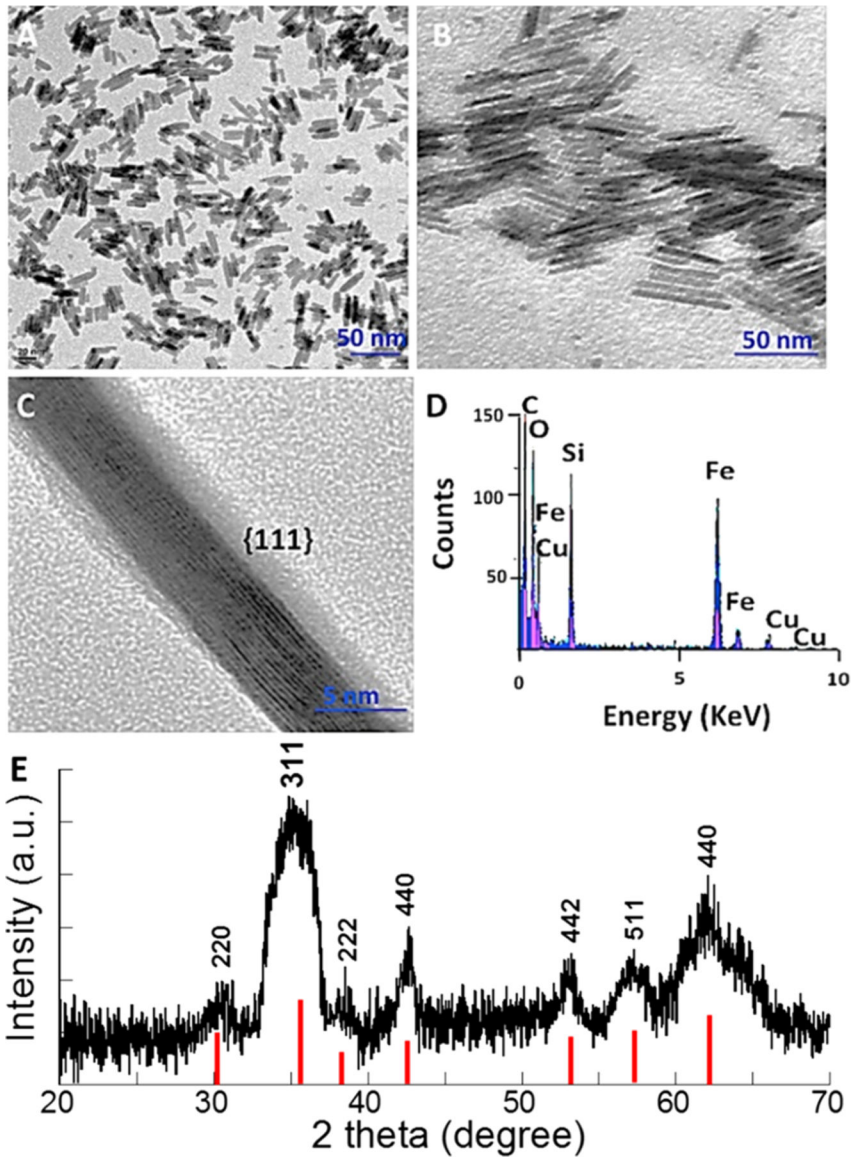

Figure 1.

TEM images of IONRs of 5 nm in diameter but different lengths. (A) IONRs (25 nm) synthesized in the presence of 0.025 mmol PEI; (B) IONRs (50 nm) synthesized in the presence of 0.01 mmol PEI; (C) high-resolution TEM images of the selected area showing lattice fringes of nanorods oriented to the crystallographic plane (scale bar of 5 nm); (D) the elements presented in the surface-coated IONRs measured by EDS, noting the Si peak coming from the TSP used for surface coating; and (E) the XRD spectrum for 50 nm long IONRs with solid red lines indicating the XRD reference pattern for magnetite.

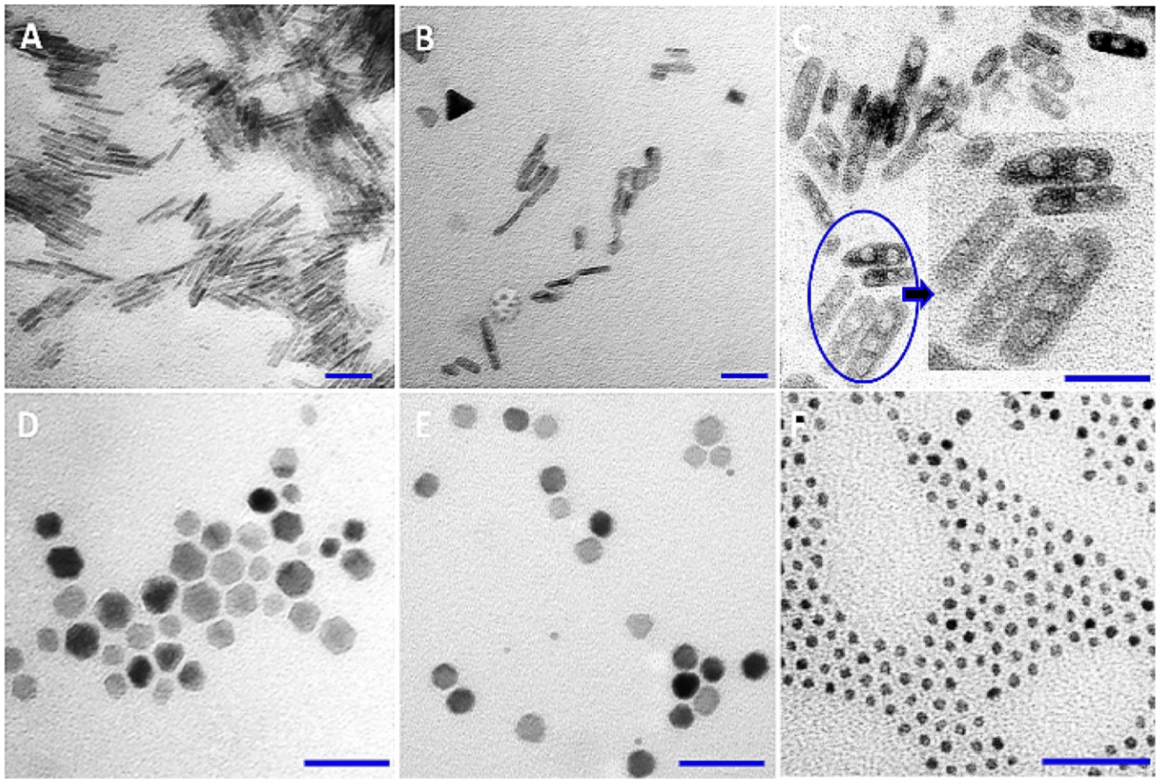

Figure 2.
TEM images of the examples of iron oxide crystals with various shapes. The shapes and morphologies of these materials were obtained by modulating: reaction temperature (A, B), reaction time (C), and oleylamine concentration (D–F). The scale bar is 50 nm.

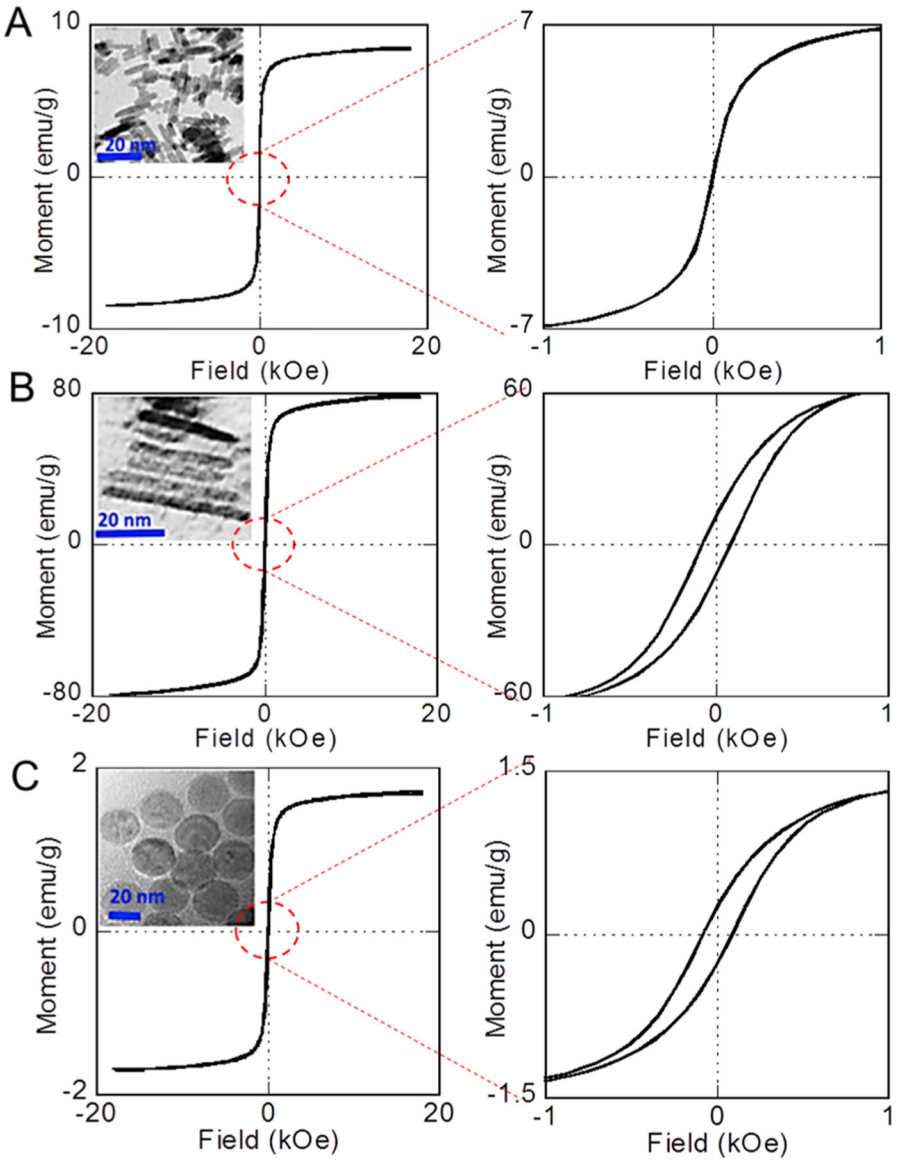

Figure 3.

Room-temperature *M–H* curves with close views of (A), 50 nm IONR (B) and 50 nm spherical IONP (C) nanoparticles. Right side: enlarged low-field regions of each *M–H* curve; insets: TEM images of each IONP or IONR.

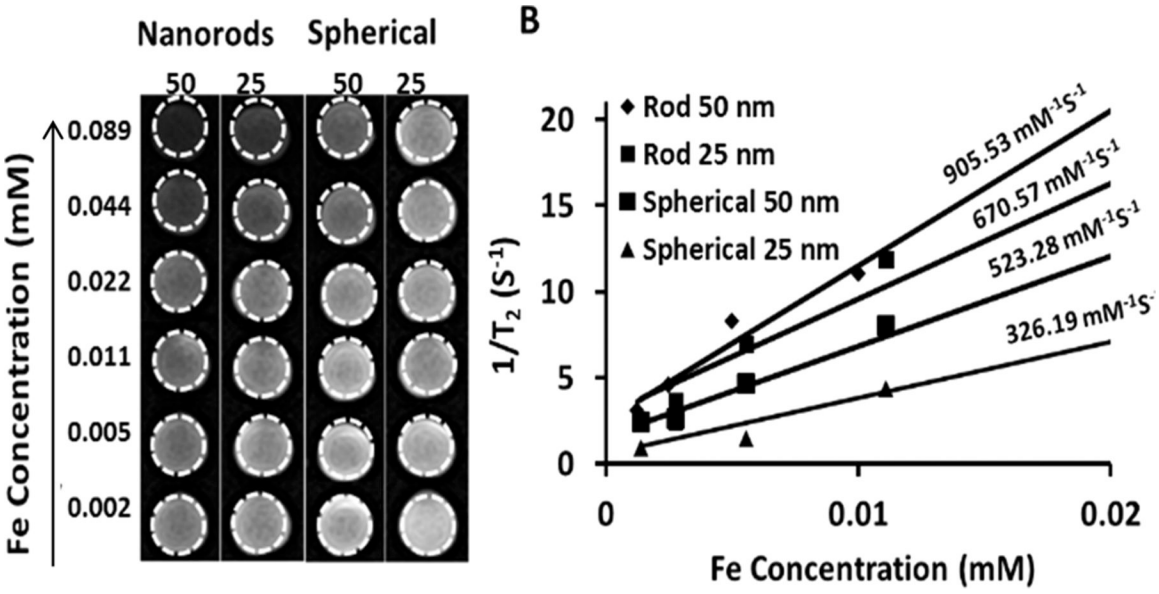

Figure 4.

T_2-weighted MR contrast effect of the IONRs at two different lengths (25 and 50 nm) and spherical IONP of two different diameters (25 and 50 nm). (A) T_2-weighted MR images of IONRs and spherical IONPs at various iron concentrations (right); (B) plots of $1/T_2$ (R_2) values of both the nanorods and spherical nanoparticles of different sizes. The corresponding relaxation rates ($r_2 = 1/T_2$) demonstrated a linear correlation with Fe concentration (B).

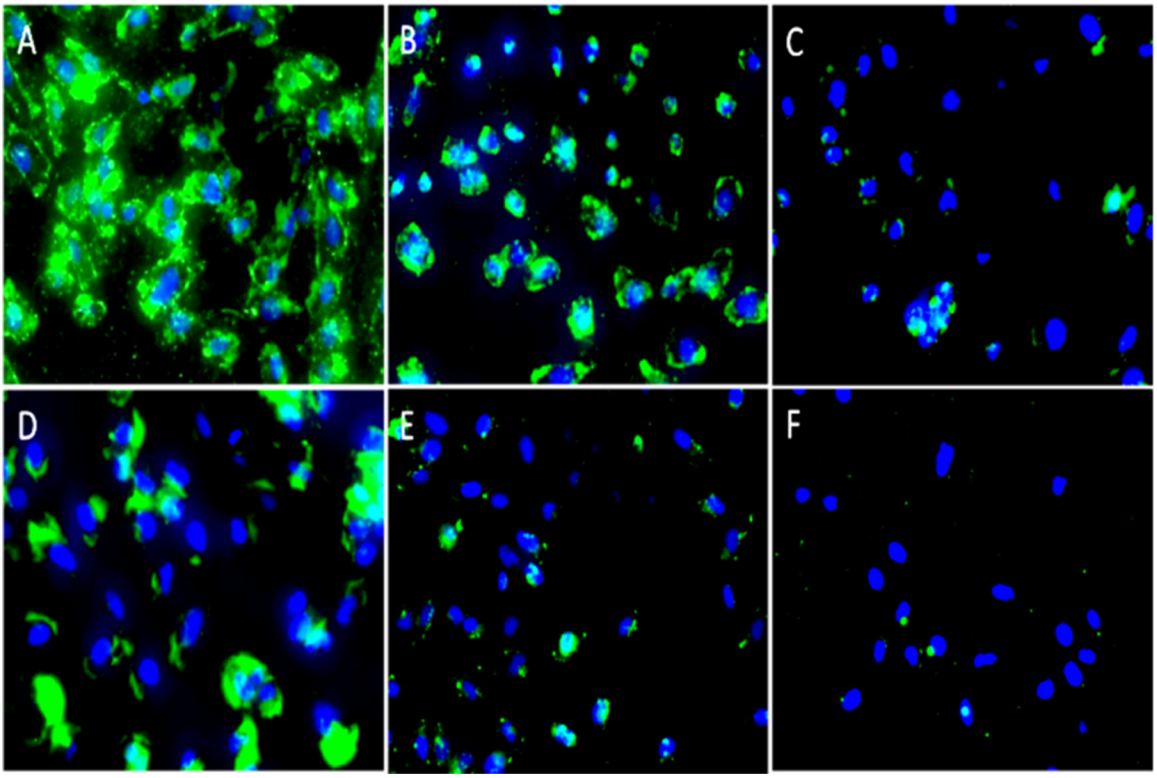

Figure 5.

Fluorescence images of the D556 medulloblastoma cells treated with different nanoparticle conjugates. Upper panels: Cells treated with nanorod conjugates Tf-IONRs (A) and BSA-IONRs (B) and cells pretreated with a fixed amount of Tf, followed by treatment with Tf-IONRs (C, blocking control experiment). Lower panel: Cells treated with spherical Tf-IONPs (D); cells treated with spherical BSA-IONPs (E); and cells pretreated with a fixed amount of Tf, followed by treatment with Tf-IONPs (F, blocking control experiment). Magnification: 20×. FITC was used to label Tf or BSA. DAPI (blue) was used to stain cell nuclei.

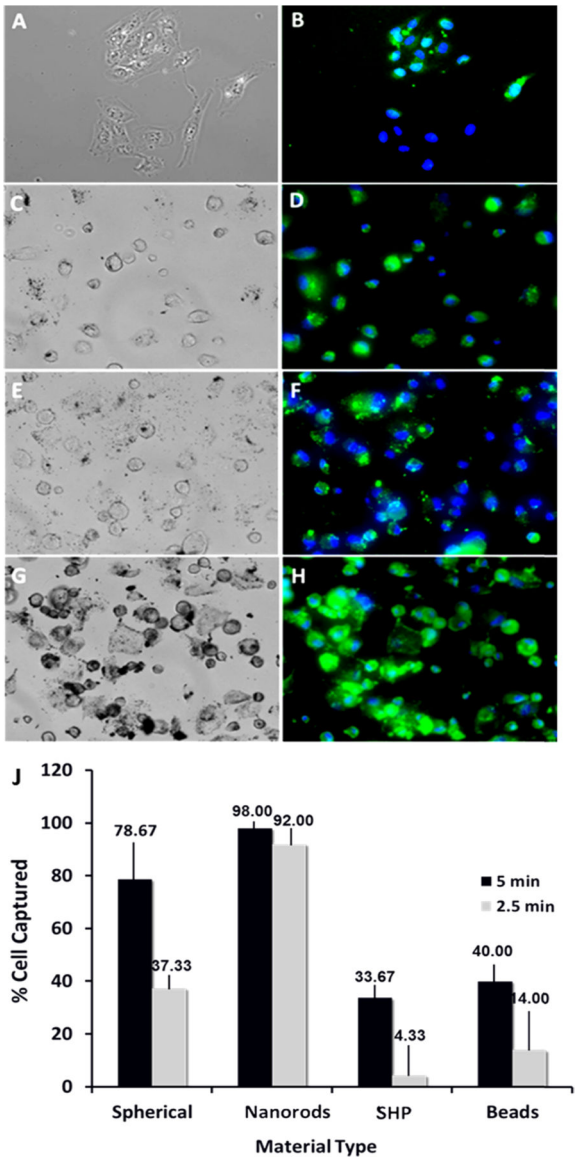

Figure 6.

Magnetic separation of medulloblastoma cancer cells using different magnetic materials. Bright light (left panel) and corresponding florescent (right) microscopy images of the captured D556 cells using: beads (commercially available Dynobeads) (A, B), SHP (commercially available IONPs) (C, D), 50 nm IONPs (E, F), 50 nm IONRs (G, H), and cell capture performance (% cell captured) of different separation reagents (I). Cell separation experiment: step 1: cells were seeded with 0.2 mg/mL IONPs for 1 h at 4 °C; step 2: cells were detached, placed in Eppendorf tubes, and diluted to 1 mL of media; step 3: cells were exposed to magnetic separation for 2.5 min and then for 5 min; step 4: the suspension containing the nontargeted cells were removed; step 5: IONPs was captured, and the separated cells were diluted in media, counted, and prepared for microscopy study.